

Self-assembly in soft matter with multiple length scales

Alberto Scacchi,^{1,2,3,*} Sousa Javan Nikkhah,² Maria Sammalkorpi,^{2,4} and Tapio Ala-Nissila^{1,5}

¹*Interdisciplinary Centre for Mathematical Modelling and Department of Mathematical Sciences, Loughborough University, Loughborough, Leicestershire LE11 3TU, UK*

²*Department of Chemistry and Materials Science,*

Aalto University, P.O. Box 16100, 00076 Aalto, Finland

³*Department of Applied Physics, Aalto University, P.O. Box 11000, FI-00076 Aalto, Finland*

⁴*Department of Bioproducts and Biosystems, Aalto University, P.O. Box 16100, FI-00076 Aalto, Finland*

⁵*Quantum Technology Finland Center of Excellence and Department of Applied Physics, Aalto University, P.O. Box 11000, FI-00076 Aalto, Finland*

(Dated: December 23, 2024)

Spontaneous self-assembly in molecular systems is a fundamental route to both biological and engineered soft matter. Simple micellisation, emulsion formation, and polymer mixing principles are well understood. However, the principles behind emergence of structures with competing length scales in soft matter systems remain an open question. Examples include the droplet-inside-droplet assembly in many biomacromolecular systems undergoing liquid-liquid phase separation, analogous multiple emulsion formation in oil-surfactant-water formulations, and polymer core-shell particles with internal structure. We develop here a microscopic theoretical model based on effective interactions between the constituents of a soft matter system to explain self-organization both at single and multiple length scales. The model identifies how spatial ordering at multiple length scales emerges due to competing interactions between the system components, e.g. molecules of different sizes and different chemical properties. As an example of single and multiple-length-scale assembly, we map out a generic phase diagram for a solution with two solute species differing in their mutual and solvent interactions. By performing molecular simulations on a block-copolymer system, we further demonstrate how the phase diagram can be connected to a molecular system that has a transition from regular single-core polymer particles to multi-core aggregates that exhibit multiple structural length scales. The findings provide guidelines to understanding the length scales rising spontaneously in biological self-assembly, but also open new venues to the development and engineering of biomolecular and polymeric functional materials.

I. INTRODUCTION

Self-assembly is Nature's ingenious route to create new materials with complex structural and functional properties. Examples range from biological self-assembly, such as protein assemblies [1], cellular condensates [2], viruses [3], or cell membranes and their internal structure, such as lipid rafts [4, 5], to widely used systems emerging from, e.g., polymer self-assembly [6–8], molecular crystals [9, 10] or bioinspired approaches to materials engineering [1, 11]. Particularly fascinating self-assembly materials are those exhibiting multiple length scales in their spatial arrangement. Examples include hierarchical biological and bioinspired materials, such as bone, nacre or crustacean exoskeletons [5], and silk-like materials [12], all featuring exceptional toughness and resilience. Many block-copolymer systems [8], coacervate droplets in biocondensates (liquid-liquid phase-separation in biological systems) [2, 13] and multiple emulsions [14] readily exhibit hierarchical multiple length scales when they self-assemble. This associates with locally varying molecular environments in terms of density and confinement, dielectric properties, or hydrophobicity and hydrophilicity, granting access to fascinating applications in nanopho-

tonics [10, 15, 16], organic electronics [10, 17], confined catalysis [18, 19], energy materials [11] and sensors [10, 16, 18]. Another important field of application is that of pharmaceutical materials and drug delivery [8, 16, 18], where the heterogenous, often compartmentalized, solvation environment is interesting for sequential delivery of multiple drug species, for instance in cancer therapy [20, 21].

Simple molecular self-organization, such as aqueous micellization and emulsion formation can be easily explained at the level of the interplay between water entropy, the relevant surface tensions, and the corresponding free energies [22]. Multiple length scales in the self-assembled structures emerge in the presence of competing interactions [8, 23]. However, fundamental theoretical underpinning is needed to understand the latter phenomenon. In this work we present a theoretical framework demonstrating how competition between molecular interactions can lead to spontaneous formation of structurally complex self-assembly matter that shows such multiple-length-scale structural features. The corresponding mapping and its connections to a block-copolymer system facilitate guidelines to molecular engineering principles for self-assembly materials.

The key insight to resolving self-assembly beyond simple single-length-scale aggregation emerges from the interplay between the effective interactions of the different constituents in the system. By modeling the interactions

* alberto.scacchi@aalto.fi

via a free-energy potential, the spatially varying average density of each component in the thermodynamic equilibrium can be obtained from energy minimization principles based on classical density functional theory (DFT) here [24–27]. This approach provides a generic phase diagram exhibiting the variety of possible equilibrium assembly configurations as a function of the system composition. We present here a formulation that covers both the formation of simple phases and a phase with multiple periodicity. The latter is commensurate with e.g. formation of droplets inside droplets such as biomolecular condensates [2] or multicore polymer micelles [28–31] and the other complex structures mentioned above. In order to demonstrate how the DFT model connects to molecular level self-assembly, we present a comparison to self-assembled phases obtained from dissipative particle dynamics (DPD) simulations [32–35] of a two component block-copolymer system in solvent.

II. THEORETICAL MODEL

For computational efficiency we focus here on a two-dimensional (2D) model of a system composed of two different species in a solvent such as water. The system is characterized by soft interactions, where the effective pair potentials between the coarse-grained complex molecules constituting the species, are designed using the generalized exponential model of index n (GEM- n). Such potentials have been extensively used to successfully describe the effective interactions in a vast variety of polymeric systems [36–43]. It is worth pointing out that the theory developed here applies generally to any molecular system that has three partially immiscible components. One of the components is considered here as the solvent, and it is implicitly present in the interaction potentials of the two explicit species. Such partially immiscible three-component systems are very common in e.g. aqueous polymer mixtures, biomolecular assemblies, colloidal systems, emulsions, and various liquid-crystal-forming systems. Although formulated here for 2D, the same formalism is valid in 3D with no loss of generality.

The statistical distribution of the average number density $\rho(\mathbf{r})$ is obtained using DFT [24–27] with the Ramakrishnan-Yussouff (RY) approximation [44] (details in the Supplementary Information (SI)). The fundamental condition for thermal stability of any self-assembled structure is that it corresponds to a minimum in the relevant thermodynamic potential. In order to achieve this for our model system, we choose a mixture formed by big (b) and small (s) particles. We model the effective interaction potential between pairs of coarse-grained particles as

$$\begin{aligned}\phi_{bb}(r) &= \varepsilon_{bb}e^{-(r/R_{bb})^4}; \\ \phi_{bs}(r) &= \varepsilon_{bs}e^{-(r/R_{bs})^2} + \varepsilon_{bs}^+e^{-\frac{1}{2}r/R_{bs}}; \\ \phi_{ss}(r) &= \varepsilon_{ss}e^{-(r/R_{ss})^8},\end{aligned}\quad (1)$$

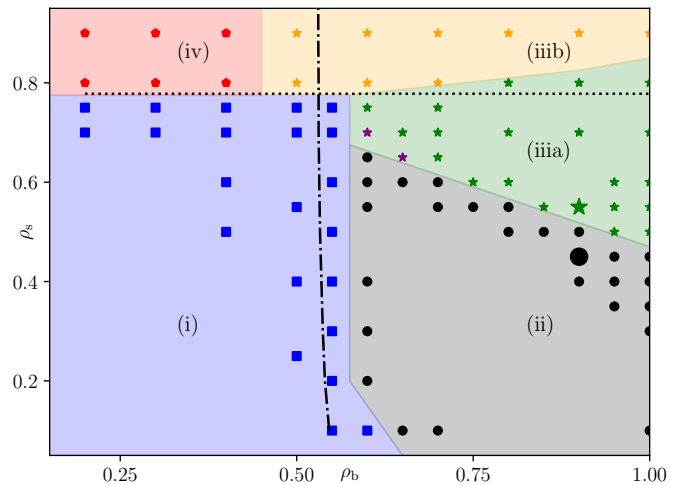


FIG. 1. Generic assembly phase diagram resulting from the 2D model binary system examined in this work. Four distinct phases emerge: (i) a phase where both b and s particle densities are spatially uniform (blue squares), (ii) a phase corresponding to one species condensing into droplets surrounded by the other species, i.e. a single-core micelle phase (black dots) (see Fig. 3 for the density profile corresponding to the large dot), (iii) a multi-length-scale phase (stars) in which the species assemble into droplets inside droplets with the response corresponding to two subsets: (iiia) multi-core micelle type assembly (see Fig. 2 for the density profile corresponding to the large star) where each s island is clearly separate from the other s islands and (iiib) where the s islands overlap at their outskirts regions, and finally (iv) a phase in which the s particles form a periodic hexagonal lattice covering the whole space while the b particles are homogeneously spread (red rhombi). This corresponds to species b being soluble while s forms droplets. Purple stars are hybrid cases. Most of the islands of s particles behave as the states corresponding to the green stars. However, some random clusters do not display the short spacing and the distribution of the s particles is similar to the one of the b particles (see Fig. 2(a)). The dotted line represents the linear instability of the length scale associated with the s particles, k_s , and the dashed-dotted line the linear instability of the length scale associated with the b particles, k_b . The boundary lines between the regions are guides to the eye.

where the subscript pairs refer to the interacting particle types, and $\varepsilon_{bb} > 0$ and $\varepsilon_{ss} > 0$ represent repulsion between pairs of b and s particles, respectively, corresponding to energy penalty for overlap due to entropic effects. ε_{bs} can be tuned to impose an attraction between b and s, and r is the distance between the centers of the particles. In water solutions, such an effective attraction typically rises between hydrophobic components as a result of entropic contributions. It could also be generated by charge distributions on the molecules. We note that for charged species, such as polyelectrolytes, this interaction can be easily tuned by salt. A long tail repulsion $\varepsilon_{bs}^+ > 0$ is useful in preventing a catastrophic assembly (singularity). R_{bb} and R_{ss} define the sizes of the particles (typically comparable to $R_{g,i}$, the radius of

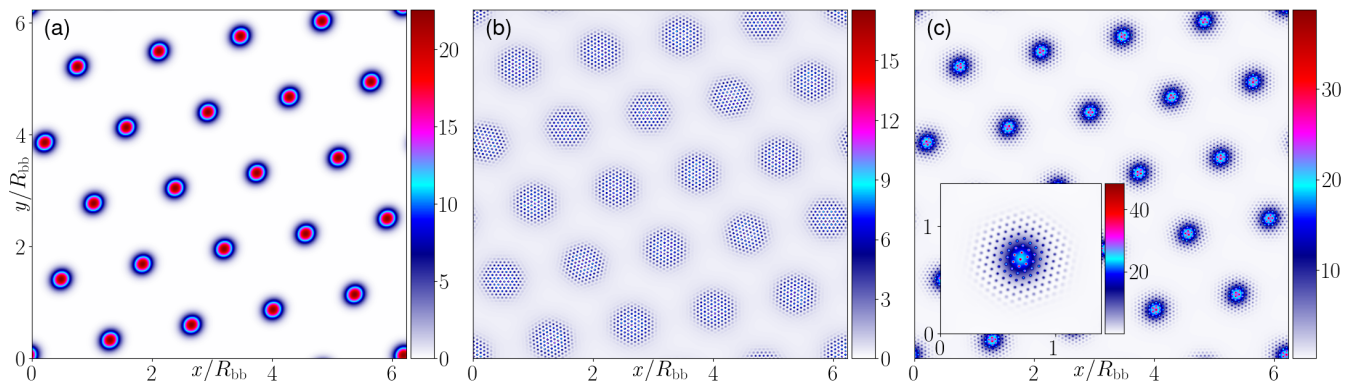


FIG. 2. Example of a dual-length-scale self-assembled phase marked by the large green star in Fig. 1. For a polymer system, this refers to multi-core micelle formation and for an emulsion to a thermodynamically stable droplet-inside-droplet state (multiple emulsion). Panel (a) has density of species b with bulk density $\rho_b^0 = 0.9$, panel (b) density of species s with bulk density $\rho_s^0 = 0.55$, and in panel (c) the total density $\rho_t(\mathbf{r}) = \rho_b(\mathbf{r}) + \rho_s(\mathbf{r})$. The density of species b forms an hexagonal structure with spacing $\approx R_{bb}$. At the same locations of these peaks, the s particles form smaller hexagonal clusters with spacing $\approx R_{ss}$. The inset shows a blow-up of a single peak.

gyration of polymer species $i = b, s$). Similar theoretical approaches have been used to describe other forms of self-assembly, such as superlattice structures [45] and quasicrystals [46].

In order to choose a physically relevant set of parameters in Eq. (1), one should direct the attention on the linear dispersion relation branches $\omega_{\pm}(k)$ derived in Ref. [47], which characterises the growth or decay of density modulations with wave number k in the liquid state. The dependence of this quantity with the different parameters in Eq. (1) is rather complicated. Before investigating such a complex quantity, we start by assuming that the mixture is formed by two independent components. This can be done by carefully selecting the interaction potentials. In order to have two clearly distinct length scales we set the ratio $k_s/k_b \approx 20$, where k_s and k_b correspond to the large and small particle characteristic wave lengths, respectively. Without loss of generality, we thus choose the radii of the particles as $R_{bb} = 5$ and $R_{ss} = 0.25$ and use dimensionless units throughout. The linear dispersion relation for a single component system is given by [48–52]

$$\omega_i(k) = -\frac{k^2 D_i}{S_i(k)}, \quad i = b, s; \quad (2)$$

where D_i is the diffusion coefficient and $S_i(k)$ the liquid structure factor of component i . It can be measured in experiments, but is also easily accessible through $S_i(k) = 1/(1 - \rho_i \hat{c}_i(k))$ [26], where $\hat{c}_i(k)$ is the Fourier transform of the direct pair correlation function (see SI for details) and ρ_i is the bulk density of species i . With this approach one can easily obtain the values of the repulsion parameters ε_{ii} necessary to achieve linear instability, for a given critical value of densities ρ_i^c , $i = b, s$, and vice versa. It is convenient (but not mandatory) to fix the values of the bulk average densities of the two species in the system to be similar, i.e. $\rho_b \approx \rho_s$. We

$\beta\varepsilon_{bb}$	$\beta\varepsilon_{bs}$	$\beta\varepsilon_{bs}^+$	$\beta\varepsilon_{ss}$	R_{bb}	R_{bs}	R_{ss}
0.45	-0.45	0.02	70	5	3	0.25

TABLE I. Set of dimensionless parameters used in Eq. (1).

choose $\beta\varepsilon_{bb} = 0.45$ and $\beta\varepsilon_{ss} = 70$, where $\beta = 1/(k_B T)$, k_B being the Boltzmann constant and T the temperature of the system. This choice implies that under the hypothesis of two independent particle systems, the critical densities are $\rho_b^c \approx 0.55$ and $\rho_s^c \approx 0.78$. These values are obtained by finding the corresponding bulk densities equivalent to the onset of linear instability in Eq. (2), i.e. for which $\omega_i(k) = 0$ and $d\omega_i(k)/dk = 0$. A common choice for the cross interaction radius is $R_{bs} = \frac{1}{2}(R_{bb} + R_{ss}) \approx 3$. In order to avoid a singularity in the density distribution, one should restrict to $2\pi \int_0^\infty dr r \phi_{bs}(r) > 0$, i.e. to a positive integrated strength of the cross-interaction. However, negative values of the integrated strength can be compensated by the strength of repulsion arising from $\phi_{bb}(r)$ and $\phi_{ss}(r)$. In addition, the attractive part of $\phi_{bs}(r)$ should be strong enough to favor mixing, and the repulsive part must be small enough to avoid phase separation. Here we choose $\beta\varepsilon_{bs} = -0.45$ and $\beta\varepsilon_{bs}^+ = 0.02$. Designing the potentials in Eq. (1) with the conditions provided above allows us to have a binary mixture in which the value of the bulk density of species i does not influence the critical bulk density of species j , for $i \neq j$. This property is evident in the fact that the instability lines in the phase diagram of Fig. 1 (to be explained in detail below) are almost vertical and horizontal, respectively. This condition is not required; however, it is very helpful in avoiding complications due to the interplay of the cross-interaction potential in $\omega_{\pm}(k)$. In fact, under some conditions this interplay could partially or fully suppress one or both instabilities. The model parameters used in Eq. (1) are summarized in Table 1. At this point it is important to emphasize that results sim-

ilar to those obtained here are to be expected for many different parameter sets in the case modeled by Eq. (1).

III. RESULTS

To facilitate comparison with computer simulations on multicomponent polymer systems in a solvent, we adopt here terminology specific to polymer self-assembly. In our theory, the linear dispersion relation contains all the information required to determine whether or not the uniform liquid is stable with respect to any perturbation defined by the wave number k . Thus, to resolve thermodynamically stable states where also assemblies with multiple length scales emerge, we address the full linear dispersion relation $\omega_{\pm}(k)$ [47] and look for the crossing point of the two linear instability lines (dashed and dashed-dotted lines in Fig. 1). For the system considered here, these two lines are almost horizontal and vertical, respectively, as mentioned previously. In this case we could have used Eq. (2) to approximate the crossing point of the two linear instability lines, but in general $\omega_{\pm}(k)$ provides the correct information. Unfortunately, knowing this crossing point gives only an idea on the values of ρ_b and ρ_s that can potentially exhibit an equilibrium structure corresponding to a multi-core state. However, this information is useful since it gives a good guideline for exploring the phase space of the system.

As already stated, we use DFT to obtain equilibrium states. The configurations provided by the theory correspond to density distribution that minimize the statistical grand canonical potential energy. The full assembly phase diagram, Fig. 1, based on the effective interactions in Eq. (1) and the set of parameters in the Table I, are obtained by varying the bulk densities ρ_b^0 and ρ_s^0 . An extensive description of this process can be found in the SI. The phase diagram consist of four distinct phases: (i) a phase where both densities are spatially uniform (blue squares); (ii) a core-shell (or single core) micelle phase (black dots); (iii) a multi-length-scale phase (stars), composed by two subsets (iiia) and (iiib); and finally (iv) a phase in which the s particles form a periodic hexagonal lattice covering the whole space while the b particles are homogeneously spread (red rhombi). We describe hereafter the different states in detail and provide physical explanation for the most interesting transitions. It is worth noting that the boundary lines between the different states in Fig. 1 are only meant to be a guide for the eye, and should not be considered as exact.

For the purpose of the present work we start the description of the different phases with the most interesting case commensurate with multi-core-micelle states in polymer assemblies, subset (iiia). An example of this structure is shown in Fig. 2 corresponding to the point marked by the large green star in Fig. 1. Here the b particles form a periodic hexagonal structure with a lattice spacing of $\approx R_{bb}$ as shown in panel (a) of Fig. 2. Simul-

taneously, the s particles form islands of small hexagonal clusters with lattice spacing $\approx R_{ss}$ centered at the density maxima of b (see panel (b) of Fig. 2). An important aspect is that the orientations of the s islands are independent of each other at each b maximum. Thus, the s particles are locally ordered within each b maximum only. This is exactly what is required to describe complex ordered phases such as multi-core micelles or multi-emulsions. We note that the perfect hexagonal order here is due to the periodic boundary conditions and lack of thermal fluctuations in the present calculations.

The structural change from states in (iiia) to states in (iiib) consists in the increase of the size of the s particles islands shown in panel (b) of Fig. 2. Increasing the density of the s particles will cause an eventual bridge between islands which are eventually not discernible. Since every array has a different orientation, grain boundaries will emerge where the various hexagonal structures meet. We mark these states with at least two islands touching each other with orange stars. The extreme case is a structure where the s particles fill completely the space (large values of ρ_s). The boundary line between orange stars and green star is meant to set an upper limit for ρ_s for which one can discern the different islands of s clusters.

On the other hand, decreasing the density of the s particles, starting from states in (iiia), causes the hexagonal arrangement of small islands s to melt to form large s droplets centered around the maxima of the b particles. However, the attractive nature of the cross-interaction potential ϕ_{bs} forces the s particles to remain in the vicinity of the maxima of b (see Fig. 3(b) and inset of Fig. 3(c) for an example corresponding to the large black circle in Fig. 1). This transition corresponds to moving from phase (iii) to phase (ii). The latter structure is commensurate with single-core or core-shell micelles. These states mostly survive for decreasing ρ_s unless the value of $\rho_b < \rho_b^c$. The phase diagram shows that multi-core micelles are obtained for the vast majority of cases for values of density $\rho_s < \rho_s^c$, i.e. for densities at which the system is linearly stable with respect to the large wave number k_s (i.e. short length scale in real space). The deviation of the actual phase boundaries from the linear instability line can be explained as follows; consider a single-core-micelle state: if the average density of the s particles in each of these peaks is roughly of the same order as the bulk threshold for instability ρ_s^c , the s particles find energetically favourable to form clusters with typical spacing on the order of $2\pi/k_s$ ((ii) \rightarrow (iii)). This can be seen as a local instability occurring at the level of a single b site.

The two purple stars in (iiia) represent state points in which most of the clusters of the s particles behave as in the case represented by green stars (see Fig. 2(b)). In these state points some random clusters of s particles do not display the short length scales and their distribution is similar to the one of the b particles (Gaussian-like distributed) (see Fig. 2(a)). These particular cases might be long-living metastable states due to the vicinity with

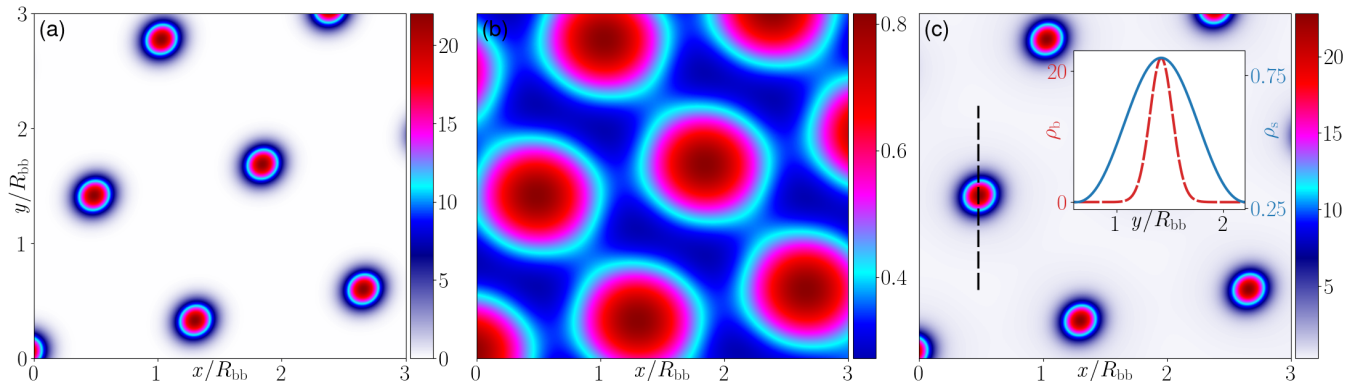


FIG. 3. Example of a single-length-scale self-assembled phase marked by the large black circle in Fig. 1. This configuration corresponds to regular polymer micelles, i.e. core-shell or core-corona configuration in polymer systems, or a standard, thermodynamically stable emulsion in which one of the species forms droplets in the carrier phase. Panel (a) has density of species b with bulk density $\rho_b^0 = 0.9$, panel (b) density of species s with bulk density $\rho_s^0 = 0.45$ and in panel (c) the total density $\rho_t(\mathbf{r}) = \rho_b(\mathbf{r}) + \rho_s(\mathbf{r})$. The inset shows a density profile cut through the dashed line in panel (c) at $x = 0.476R_{bb}$. The solid (blue) line represents the density of the s particles and the dashed (red) line the (much larger) density of the b particles. The size of the system is $6.22R_{bb} \times 6.22R_{bb}$.

State	i	ii	iii	iv
ρ_b	const.	hex R_{bb}	hex R_{bb}	const.
ρ_s	const.	hex R_{bb}	hex islands R_{ss} on top of hex R_{bb}	hex R_{ss}

TABLE II. Summary of the symmetries of ρ_b and ρ_s in the different phases.

the phase boundaries.

The (red) rhombi, i.e. phase (iv), represent states where the whole system is filled by a periodic hexagonal structure with the typical spacing characteristic of the s particles, i.e. $\approx R_{ss}$. Simultaneously, the b particles are homogeneously spread over the system. This region can be found for large values of $\rho_s > \rho_s^c$ and for small values of $\rho_b < \rho_b^c$. The attractive nature of the cross-interaction potential favours the orange-star states to exist down to values of $\rho_b < \rho_b^c$, at which one would expect to find rhombi states if only linear instabilities are considered. Cluster formation of b particles is enhanced by the attraction mediated by clusters of s particles. This can be explained in a manner similar to the discrepancy between the linear instability line of the s particles and the boundary between black circles and the green stars. Finally, the (blue) squares, phase (i), represent states in which both species are in a homogeneous state, i.e. a solution of miscible species. One can appreciate a slight discrepancy between the linear instability line of particles b and the boundary between the liquid state and the states in which the latter species is linearly unstable. This is due to finite-size effects and also to the fact that the dispersion relation does not consider the non-linear contributions to the full dynamics. The size of the system has been chosen randomly, thus, it might not favour hexagons with the expected lattice spacing. The box selects a wave number slightly different from k_b . The linear

dispersion relation in the vicinity of k_b is concave with a maximum at $\approx k_b$ (exactly k_b at the onset of the linear instability), thus the b particles will form a cluster crystal structure for a slightly higher value of ρ_b , consequently a slightly different typical spacing.

A summary of the symmetries of ρ_b and ρ_s in the four different phases in Fig. 1 is reported in Table II. We note that the transition between phases (ii) and (iii) is discontinuous. This is due to spatial symmetry breaking between these two phases. A comparison with particle based simulations of a polymer mixture of this phase transition is presented in the next section.

IV. DISSIPATIVE PARTICLE DYNAMICS SIMULATIONS

To compare how single vs. multiple length scale assembly emerges in a realistic molecular level system, we have performed dissipative particle dynamics (DPD) [34, 35] simulations of a polymeric solution composed of a solvophobic polymer (A_{19}) and a di-block copolymer (A_1B_6) in a solvent (W) using the LAMMPS [53] simulation package. The segments A and B are solvophobic and solvophilic, respectively, and the subscripts refer to the number of DPD beads (block lengths). Each DPD bead represents a group of atoms which experience a force $\mathbf{F}_i = \sum_{j \neq i} \mathbf{F}_{ij}^C + \mathbf{F}_{ij}^D + \mathbf{F}_{ij}^R$, $i, j = 1, \dots, N$, where \mathbf{F}^C describes conservative interactions, \mathbf{F}^D dissipative contributions, \mathbf{F}^R the random contribution, and N corresponds to the number of beads in the system. The interaction forces are treated as pairwise additive and are truncated at a cutoff distance r_c . In the polymer chains, adjacent beads also contribute to a spring-like force \mathbf{F}^S . The soft potentials in DPD facilitate acceleration of the numerical simulations such that realistic experimental time and

length scales for block-copolymer self-assembly can be achieved. Further details regarding the method, polymer component interactions, and additional simulation specifics can be found in the SI.

In Fig. 4 we show snapshots of different equilibrium configurations obtained from DPD simulations by varying the molar fractions of the two species. The binary polymer system strikingly self-assembles into the structures shown in the two panels corresponding to a multi-core-corona and a single-core-corona or core-shell states. The two cases correspond to a total solid content of $N_s/(N_s + N_w) = 20.15\%$ in aqueous solvent, where N_s and N_w are the number of solid and water beads, respectively. In the multi-core configuration the molar fractions are 10 % of A_{19} and 90 % of A_1B_6 , and in the single-core case there is 50 % of A_{19} and 50 % of A_1B_6 . The simulations are performed in a cubic box of $100 \times 100 \times 100 r_c^3$, where r_c is the cutoff radius of the interaction between beads. These distinct equilibrium configurations show dual and single-length-scale structural assemblies analogous to those present in our DFT based phase diagram (phases (ii) and (iiia) in Fig. 1). It is tempting to interpret a DPD polymer chain as a single coarse-grained DFT particle, but it should be noted that the surfactant-like nature of the copolymer makes a quantitative comparison between the chemically predictive molecular model and the DFT assembly structures difficult. Although we cannot directly map the GEM- n interactions to those between the DPD beads, the two distinct length scales emerging from the effective interactions in Fig. 2 appear in the DPD model. Also, in the DPD simulations the key feature for multi-core assembly is a sufficient degree of immiscibility between the species. The formation of solvophobic polymer cores needs to be energetically favorable, they need to be stabilized to a sufficient degree by the solvophilic polymer segments, and the solvophilic polymer cannot have too favorable interactions with either the solvent or the solvophobic polymer. If either the solvophobic polymers are too solvophobic, or the solvophilic one too solvophilic, or the two polymers readily mix, the assembly becomes core-shell or phase separates. This demonstrates how the competition between interactions and a mutual balance of immiscibility gives rise to multiple-length-scale assemblies – single-length-scale self-assembly is retained when any of the pairwise effective interactions dominates.

V. CONCLUSIONS

While spontaneous self-assembly of multicomponent systems has important applications, it has remained poorly understood. We have here presented a microscopic theory capable of explaining this phenomenon within soft matter systems with multiple competing length scales. The theory relies on the interplay between the effective interaction potentials used to model the different constituents of a soft-matter system such

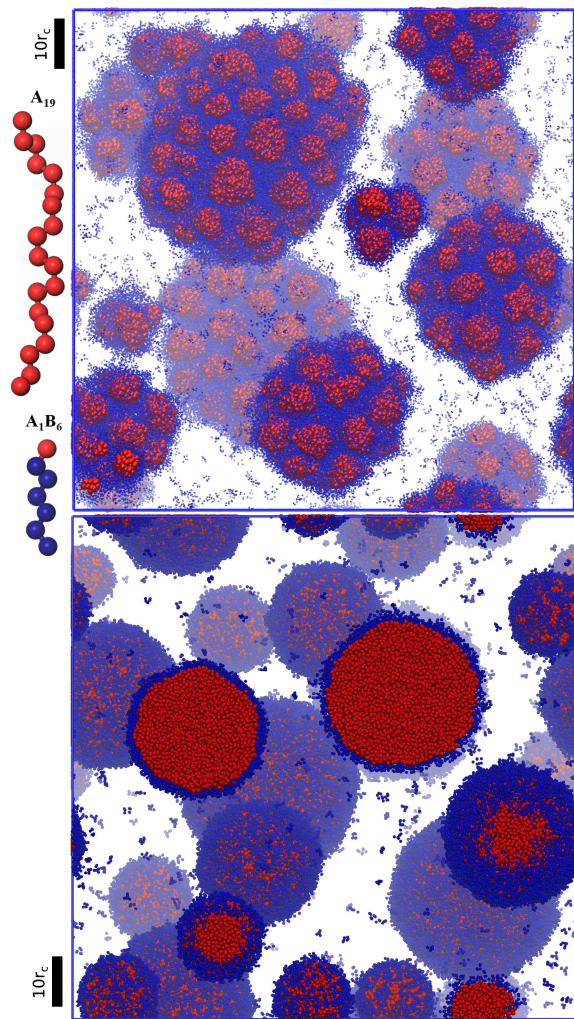


FIG. 4. Snapshots of equilibrium configurations from 3D DPD simulations of a polymeric solution composed of a solvophobic polymer (A_{19}) and a di-block copolymer (A_1B_6) in a solvent (W). The segments A (red) and B (blue) are solvophobic and solvophilic, respectively, and subscript refers to the number of DPD beads or coarse-grained particles. Top panel: multi-core configuration for a system formed of molar fractions of 10% A_{19} and 90% of A_1B_6 . Bottom panel: single-core (core-shell or core-corona) configuration for a molar fractions of 50% A_{19} and 50% of A_1B_6 . The solvent W is not shown in the visualization for clarity.

as biological and biomolecular assemblies, polymer materials, or colloids, such as vesicles, emulsions, foams, or gels. The theory enables to recognize how the multiple intrinsic length scales rise from competition between the different intrinsic length scales of the individual components and the cross-interaction attractions. We have mapped out the full phase diagram for a binary system in solvent, where both single and multi-length-scale structures emerge when the densities of the two components are varied. Analogous results are expected from systems interacting differently from the one addressed here, assuming that comparable properties govern the interplay

between the effective interaction potentials. Through the inspection of the linear dispersion relation, one can further identify or engineer the distinctive length scales in the assembled structures. This provides a handle to proposing tuning of the assemblies. Finally, we have also performed molecular simulations of a block copolymer mixture in solvent to demonstrate how simple micelles and multi-core structures emerge when molar fractions are changed. These molecular level equilibrium structures match with the morphologies predicted by the theory providing a connection to chemical nature of the assembling species.

The significance of our findings resides in the identification of the key molecular features involved in general multiple-length-scale self-assembly. Although multiple-length-scale assembly is ubiquitous, such guidelines have been lacking until now. By providing much needed insight to understanding, e.g., morphologies rising in intracellular biocondensates, multiple emulsions, or lipid bilayer microdomains, we obtain here the means to engineer and tune soft matter to desired multiple length scale structures. In addition to obvious applications to multiple length scale self-assembling compartmentalization, such as drug delivery, catalysis and selective multistep reaction platforms, our work also provides tools to harnessing the full potential of revolutionary materials pro-

duction via biological mechanisms, advanced engineered biomaterials, or complex polymer assemblies by providing crucial insight on how to tune the assembly response.

VI. ACKNOWLEDGEMENT

A.S. is thankful to Andrew J. Archer for fruitful discussions. This work was supported by Academy of Finland grants No. 309324 (M.S.) and Nos. 307806 and 312298 (T.A.-N.). We are grateful for the support by FinnCERES Materials Bioeconomy Ecosystem. Computational resources by CSC IT Centre for Finland and RAMI – RawMatters Finland Infrastructure are also gratefully acknowledged.

VII. AUTHOR CONTRIBUTIONS

This work was conceived and supervised by T.A.-N. and M.S. A.S. formulated and executed the theoretical calculations and wrote the first draft of the manuscript. S.J.N. carried out the molecular simulations. All authors contributed to writing.

-
- [1] B. J. G. E. Pieters, M. B. van Eldijk, R. J. M. Nolte, and J. Mecnović, *Chemical Society Reviews* **45**, 24 (2016).
 - [2] S. F. Banani, H. O. Lee, A. A. Hyman, and M. K. Rosen, *Nature Reviews Molecular Cell Biology* **18**, 285 (2017).
 - [3] R. Zandi, B. Dragnea, A. Travesset, and R. Podgornik, *Physics Reports* **847**, 1 (2020).
 - [4] E. Sezgin, I. Levental, S. Mayor, and C. Eggeling, *Nature Reviews Molecular Cell Biology* **18**, 361 (2017).
 - [5] M. A. Meyers, P.-Y. Chen, A. Y.-M. Lin, and Y. Seki, *Progress in Materials Science* **53**, 1 (2008).
 - [6] M. A. Cohen Stuart, W. T. Huck, J. Genzer, M. Müller, C. Ober, M. Stamm, G. B. Sukhorukov, I. Szleifer, V. V. Tsukruk, M. Urban, *et al.*, *Nature Materials* **9**, 101 (2010).
 - [7] L. MacFarlane, H. Shaikh, J. Garcia-Hernandez, M. Vespa, T. Fukui, and I. Manners, *Nature Reviews Materials* (2020).
 - [8] Y. Lu, J. Lin, L. Wang, L. Zhang, and C. Cai, *Chemical Reviews* **120**, 4111 (2020).
 - [9] I. I. Smalyukh, *Annual Review of Condensed Matter Physics* **9**, 207 (2018).
 - [10] K. R. Phillips, G. T. England, S. Sunny, E. Shirman, T. Shirman, N. Vogel, and J. Aizenberg, *Chemical Society Reviews* **45**, 281 (2016).
 - [11] C. Gong, S. Sun, Y. Zhang, L. Sun, Z. Su, A. Wu, and G. Wei, *Nanoscale* **11**, 4147 (2019).
 - [12] Y. Wang, J. Guo, L. Zhou, C. Ye, F. G. Omenetto, D. L. Kaplan, and S. Ling, *Advanced Functional Materials* **28**, 1805305 (2018).
 - [13] T. Lu and E. Spruijt, *Journal of the American Chemical Society* **142**, 2905 (2020).
 - [14] T. Sheth, S. Seshadri, T. Prileszky, and M. E. Helgeson, *Nature Reviews Materials* , 1 (2020).
 - [15] L.-L. Ma, W. Hu, Z.-G. Zheng, S.-B. Wu, P. Chen, Q. Li, and Y.-Q. Lu, *Advanced Optical Materials* **7**, 1900393 (2019).
 - [16] M. Qi and Y. Zhou, *Materials Chemistry Frontiers* **3**, 1994 (2019).
 - [17] S. Casalini, C. A. Bortolotti, F. Leonardi, and F. Biscarini, *Chemical Society Reviews* **46**, 40 (2017).
 - [18] M. York-Duran, M. Godoy-Gallardo, C. Labay, A. Urquhart, T. Andresen, and L. Hosta-Rigau, *Colloids and Surfaces B: Biointerfaces* **152**, 199 (2017).
 - [19] J. Gaitzsch, X. Huang, and B. Voit, *Chemical Reviews* **116**, 1053 (2016).
 - [20] M. S. Aw, M. Kurian, and D. Losic, *Chemistry - A European Journal* **19**, 12586 (2013).
 - [21] M. Wu, Y. Zhu, and W. Jiang, *Angewandte Chemie International Edition* **57**, 3578 (2018).
 - [22] R. Nagarajan and E. Ruckenstein, *Langmuir* **7**, 2934 (1991).
 - [23] V. Palermo and P. Samorì, *Angewandte Chemie International Edition* **46**, 4428 (2007).
 - [24] J.-P. Hansen and I. R. McDonald, eds., *Theory of Simple Liquids*, 4th ed. (Academic Press, Oxford, UK, 2013).
 - [25] R. Evans, *Advances in Physics* **28**, 143 (1979).
 - [26] R. Evans, “Density functionals in the theory of non-uniform fluids,” in *Fundamentals of Inhomogeneous Fluids*, edited by D. Henderson (1992) pp. 85 – 175.
 - [27] J. F. Lutsko, *Advances in chemical physics* **144**, 1 (2010).
 - [28] H. Chen and E. Ruckenstein, *Langmuir* **29**, 5428 (2013).

- [29] N. Duxin, F. Liu, H. Vali, and A. Eisenberg, *Journal of the American Chemical Society* **127**, 10063 (2005).
- [30] M. Ueda, A. Hashidzume, and T. Sato, *Macromolecules* **44**, 2970 (2011).
- [31] H. Chen and E. Ruckenstein, *Soft Matter* **8**, 8911 (2012).
- [32] P. Hoogerbrugge and J. Koelman, *Europhysics Letters* **19**, 155 (1992).
- [33] P. Espanol and P. Warren, *Europhysics Letters* **30**, 191 (1995).
- [34] R. D. Groot and P. B. Warren, *Journal of Chemical Physics* **107**, 4423 (1997).
- [35] P. Español and P. B. Warren, *Journal of Chemical Physics* **146**, 150901 (2017).
- [36] P. Bolhuis, A. Louis, J. Hansen, and E. Meijer, *Journal of Chemical Physics* **114**, 4296 (2001).
- [37] C. N. Likos, *Physics Reports* **348**, 267 (2001).
- [38] C. Likos, H. Löwen, M. Watzlawek, B. Abbas, O. Jucknischke, J. Allgaier, and D. Richter, *Physical Review Letters* **80**, 4450 (1998).
- [39] A. Louis, P. Bolhuis, J. Hansen, and E. Meijer, *Physical Review Letters* **85**, 2522 (2000).
- [40] I. Götze, H. Harreis, and C. Likos, *Journal of Chemical Physics* **120**, 7761 (2004).
- [41] C. N. Likos, *Soft Matter* **2**, 478 (2006).
- [42] D. A. Lenz, R. Blaak, C. N. Likos, and B. M. Mladek, *Physical Review Letters* **109**, 228301 (2012).
- [43] B. M. Mladek, D. Gottwald, G. Kahl, M. Neumann, and C. N. Likos, *Physical Review Letters* **96**, 045701 (2006).
- [44] T. V. Ramakrishnan and M. Yussouff, *Physical Review B* **19**, 2775 (1979).
- [45] W. Somerville, J. Stokes, A. Adawi, T. Horozov, A. J. Archer, and D. Buzza, *Journal of Physics: Condensed Matter* **30**, 405102 (2018).
- [46] A. Scacchi, W. Somerville, D. Buzza, and A. Archer, *Physical Review Research* **2**, 032043 (2020).
- [47] A. J. Archer, M. C. Walters, U. Thiele, and E. Knobloch, *Physical Review E* **90**, 042404 (2014).
- [48] A. J. Archer and R. Evans, *Journal of Chemical Physics* **121**, 4246 (2004).
- [49] A. J. Archer, *Journal of Physics: Condensed Matter* **18**, 5617 (2006).
- [50] A. J. Archer, A. M. Rucklidge, and E. Knobloch, *Physical Review Letters* **111**, 165501 (2013).
- [51] A. J. Archer, A. M. Rucklidge, and E. Knobloch, *Physical Review E* **92**, 012324 (2015).
- [52] M. C. Walters, P. Subramanian, A. J. Archer, and R. Evans, *Physical Review E* **98**, 012606 (2018).
- [53] S. Plimpton, *Journal of Computational Physics* **117**, 1 (1995).

Supplementary Information

Density functional theory for mixtures and the Ramakrishnan and Yussouff approximation

The grand potential of a system composed of two types of particles is

$$\Omega[\rho_1, \rho_2] = \mathcal{F}[\rho_1, \rho_2] + \sum_{i=1,2} \int d\mathbf{r} [V_i^{\text{ext}}(\mathbf{r}) - \mu_i] \rho_i(\mathbf{r}), \quad (\text{S1})$$

where \mathcal{F} is the intrinsic Helmholtz free energy functional, $\rho_1 = \rho_1(\mathbf{r})$ and $\rho_2 = \rho_2(\mathbf{r})$ are the spatially varying densities of the two species, $V_i^{\text{ext}}(\mathbf{r})$ is the one-body external potential acting on species i (for bulk systems $V_i^{\text{ext}}(\mathbf{r}) \equiv 0$ for $i = 1, 2$) and μ_i are the chemical potentials. The intrinsic Helmholtz free energy can be split into two terms

$$\mathcal{F}[\rho_1, \rho_2] = \mathcal{F}^{\text{id}}[\rho_1, \rho_2] + \mathcal{F}^{\text{exc}}[\rho_1, \rho_2], \quad (\text{S2})$$

where the first term is the ideal gas contribution, i.e.

$$\mathcal{F}^{\text{id}}[\rho_1, \rho_2] = k_{\text{B}}T \sum_{i=1,2} \int d\mathbf{r} \rho_i(\mathbf{r}) \ln(\Lambda_i^d \rho_i(\mathbf{r}) - 1), \quad (\text{S3})$$

and Λ_i is the thermal de Broglie wavelength, d is the dimensionality of the system, T the temperature and k_{B} the Boltzmann constant. The second term in Eq. (S2) is the excess Helmholtz free energy arising from the interactions between the particles. Following Ramakrishnan and Yussouff [44], we approximate this functional by a functional Taylor expansion around the homogeneous fluid states $\rho_{0,i}$. A truncation of the series expansion at second order gives

$$\mathcal{F}^{\text{exc}}[\rho_1, \rho_2] = \mathcal{F}^{\text{exc}}[\rho_{0,1}, \rho_{0,2}] + \sum_{i=1,2} \int d\mathbf{r} \mu_i^{\text{ex}} \delta\rho_i(\mathbf{r}) - \frac{1}{2\beta} \sum_{\substack{i=1,2 \\ j=1,2}} \int d\mathbf{r} \int d\mathbf{r}' \delta\rho_i(\mathbf{r}) c_{ij}(|\mathbf{r} - \mathbf{r}'|) \delta\rho_j(\mathbf{r}'), \quad (\text{S4})$$

where $\delta\rho_i(\mathbf{r}) = \rho_i(\mathbf{r}) - \rho_{0,i}$ and $\mu_i^{\text{ex}} = \mu_i - k_{\text{B}}T \ln(\rho_{0,i} \Lambda_i)$ are the excess chemical potentials. The pair direct correlation functions $c_{ij}(\mathbf{r})$ are obtained via the random phase approximation (RPA). The RPA consists of assuming a simple mean-field form for the excess free energy in Eq. (S2). This leads to $c_{ij}(\mathbf{r}) = -\beta\phi_{ij}(\mathbf{r})$, where $\phi_{ij}(\mathbf{r})$ are the effective pair potentials, and $\beta = (k_{\text{B}}T)^{-1}$ [37]. For additional accuracy, one could, for example, use the hypernetted chain (HNC) Ornstein-Zernike integral equation theory [24]. The equilibrium density profiles $\rho_i(\mathbf{r})$ are those which minimise the functional of the grand potential $\Omega[\rho_1, \rho_2]$ and which therefore satisfy the following pair of coupled Euler-Lagrange equations

$$\frac{\delta\Omega[\rho_1, \rho_2]}{\delta\rho_i} = 0, \quad (\text{S5})$$

for $i = 1, 2$.

Difference in the grand canonical potential energy

Substituting Eqs. (S2-S4) into Eq. (S1) one obtains an expression for the grand canonical potential. For homogeneous system, i.e. $\rho_1(\mathbf{r}) = \rho_{0,1}$ and $\rho_2(\mathbf{r}) = \rho_{0,2}$, the latter reduces to

$$\Omega^0[\rho_{0,1}, \rho_{0,2}] = \frac{1}{\beta} \sum_{i=1}^2 \int d\mathbf{r} \rho_{0,i} [\ln(\Lambda_i^d \rho_{0,i}) - 1 - \beta\mu_i] + \mathcal{F}^{\text{exc}}[\rho_{0,1}, \rho_{0,2}]. \quad (\text{S6})$$

The difference in the grand canonical potential energy between the equilibrium state and the corresponding homogeneous state becomes

$$\begin{aligned} \Delta\Omega = \Omega[\rho_1, \rho_2] - \Omega^0[\rho_{0,1}, \rho_{0,2}] &= \frac{1}{\beta} \sum_{i=1}^2 \int d\mathbf{r} \left[\rho_i(\mathbf{r}) \ln \left[\frac{\rho_i(\mathbf{r})}{\rho_{0,i}} \right] - \delta\rho_i(\mathbf{r}) \right] \\ &\quad - \frac{1}{2\beta} \sum_{\substack{i=1,2 \\ j=1,2}} \int d\mathbf{r} \int d\mathbf{r}' \delta\rho_i(\mathbf{r}) c_{ij}(|\mathbf{r} - \mathbf{r}'|) \delta\rho_j(\mathbf{r}'). \end{aligned} \quad (\text{S7})$$

Dissipative particle dynamics simulations (DPD)

The DPD simulation method, originally proposed by Hoogerbrugge and Koelman [34], is a mesoscale coarse-grained bead-based molecular simulation technique. Combining aspects of molecular dynamics and lattice-gas automata, DPD acknowledges the idea that different beads can overlap, modelling non-bonded interactions with soft repulsive potentials [34, 35]. The soft potentials employed to describe the interactions between the beads allow the simulations to reach realistic experimental time and length scales for e.g. block-copolymer self-assembly systems. Each DPD bead represents a coarse-grained region in the molecular system (e.g. several monomers of a polymer, or a solvent region, or a group of atoms) which experience a force

$$\mathbf{F}_i = \sum_{j \neq i} \mathbf{F}_{ij}^C + \mathbf{F}_{ij}^D + \mathbf{F}_{ij}^R, \quad i, j = 1, \dots, N, \quad (\text{S8})$$

where \mathbf{F}^C describes conservative interactions, \mathbf{F}^D dissipative contributions, \mathbf{F}^R a random contribution, and N corresponds to the number of DPD beads in the system. The interaction forces are treated as pairwise additive and are truncated at a distance r_c .

The conservative force is a soft repulsive force acting along the centers of two DPD particles, given by

$$\mathbf{F}_{ij}^C = a_{ij}(1 - r_{ij})\hat{\mathbf{r}}_{ij}, \quad (\text{S9})$$

where a_{ij} is the maximum repulsion between beads i and j , $r_{ij} = |r_i - r_j|/r_c$ is the cut-off normalized distance between beads i and j , and $\hat{\mathbf{r}}_{ij} = \mathbf{r}_{ij}/r_{ij}$ gives the force direction via a unit vector. The coefficient a_{ij} is connected to the Flory-Huggins mixing parameter χ_{ij} via the relation $\chi_{ij} = (a_{ij} - a_{ii})/3.27$ at a density $\rho = 3$. The choice $a_{ii} = 25$ for the repulsion parameter between beads of the same species (i.e., $\chi_{ii} = 0$) is common and based on the compressibility of the dilute solution [34]. An a_{ij} value exceeding the self-repulsion in magnitude corresponds to a stronger bead-bead repulsion between beads of different species.

The dissipative force is given by

$$\mathbf{F}_{ij}^D = -\gamma\omega^D(r_{ij})(\hat{\mathbf{r}}_{ij} \cdot \mathbf{v}_{ij})\hat{\mathbf{r}}_{ij}, \quad (\text{S10})$$

where γ is a viscosity related parameter ($\gamma = 4.5$), ω^D is a weight function that goes to zero at r_c , and the relative velocity is $\mathbf{v}_{ij} = \mathbf{v}_i - \mathbf{v}_j$.

The random force is given by

$$\mathbf{F}_{ij}^R = \sigma\omega^R(r_{ij})\xi_{ij}\hat{\mathbf{r}}_{ij}, \quad (\text{S11})$$

where ξ_{ij} is a zero-mean Gaussian random variable of unit variance and $\sigma^2 = 2\gamma k_B T$. The weight functions follow the relation $\omega^D(r_{ij}) = \omega^R(r_{ij})^2 = (1 - r_{ij})^2$ for $r_{ij} < r_c$. Consecutive beads in a polymer chain also perceive a spring force \mathbf{F}_i^S defined by

$$\mathbf{F}_i^S = \sum_{j^*} C r_{ij}, \quad (\text{S12})$$

where C is the spring constant, which is set to $C = 4$ in this work, and j^* refers to the nearest neighbours in the chain.

The system modelled in this work is composed of a mixture of a solvophobic polymer (A_{19}) and a di-block copolymer (A_1B_6) in a solvent (S) medium. The nomenclature A, B, S refers to the DPD beads such that A is a solvophobic bead, B a solvophilic bead and S the solvent bead. The subscripts refer to the number of beads in the chain. For the interactions between beads of same type, we use $a_{AA} = a_{BB} = a_{SS} = 25$. This value is based on the compressibility of the dilute solution [34]. The interactions between the beads in the simulations are $a_{AB} = 72$, $a_{AS} = 115$ and $a_{BS} = 30$. To simplify the DPD equations and simulations, the cutoff radius r_c , the bead mass m , and the energy $k_B T$ are reduced to $r_c = m = k_B T = 1$ which leads to the time unit $\tau = (mr_c^2/k_B T)^{1/2} = 1$.

The DPD simulations were performed using the LAMMPS [53] package. A modified version of the velocity-Verlet algorithm is used to integrate the equations of motion. A time step of $\Delta t = 0.05\tau$ is used. The simulations are performed in a cubic box of $100 \times 100 \times 100 r_c^3$ in size. Periodic boundary conditions in all directions in 3D were used. The system is initialized with setting the polymers and the solvent beads with random placement in the box (overlap excluded in initialization). The simulations were carried out for 2×10^6 time steps, and equilibration checked for via analysis of the time evolution of the assembly structures.